PSMA-PET/CT–based Lymph Node Atlas for Prostate Cancer Patients Recurring After Primary Treatment: Clinical Implications for Salvage Radiation Therapy

Kilian Schiller[a,*,†], *Lucia Stöhrer*[a,†], *Mathias Düsberg*[a], *Kai Borm*[a], *Michal Devecka*[a], *Marco M.E. Vogel*[a], *Robert Tauber*[b], *Matthias M. Heck*[b], *Isabel Rauscher*[c], *Matthias Eiber*[c], *Jürgen E. Gschwend*[b], *Marciana Nona Duma*[a,d], *Stephanie E. Combs*[a,e,f]

[a] *Department of Radiation Oncology, Technical University Munich (TUM), Munich, Germany;* [b] *Department of Urology, Technical University Munich (TUM), Munich, Germany;* [c] *Department of Nuclear Medicine, Technical University Munich (TUM), Munich, Germany;* [d] *Department of Radiation Oncology, Friedrich-Schiller University Jena, Jena, Germany;* [e] *Department of Radiation Sciences (DRS), Institute of Radiation Medicine (IRM), Helmholtz Zentrum München, Munich, Germany;* [f] *Deutsches Konsortium für Translationale Krebsforschung (DKTK), Partner Site Munich, Munich, Germany*

[†] Both authors contributed equally.
[*] Corresponding author. Department of Radiation Oncology, Technical University Munich (TUM), Munich, Germany. Tel.: +49 89 4140 4512; Fax: +49 89 4140 4882.

Introduction

Prostate cancer (PC) is one of the most common cancers affecting men worldwide, with over 1 million new cases each year, contributing to roughly 15% of all cancer diagnoses [1].

Radical prostatectomy (RP) is a successful initial treatment option for patients diagnosed with PC with different prognostic factors (eg, tumor stage [T] and patient's age). However, approximately 20–40% of patients with clinically localized PC will experience biochemical recurrence (BCR) after RP [2–4].

In this setting, salvage radiation therapy (SRT) can be a curative approach. The extent of the radiation target volume in SRT is of utmost importance, especially when suspecting nodal involvement.

When the site of recurrence is not known, the Radiation Therapy Oncology Group (RTOG) guidelines [5] for delineation of lymph node (LN) clinical target volume (CTV) is typically used.

In this case, it remains questionable whether all affected LNs are fully covered by the radiation volume. Conventional imaging technologies (computed tomography [CT] and magnetic resonance imaging) have limited potential to detect potential LN involvement reliably [6].

Over the past years, prostate-specific membrane antigen positron emission tomography (PSMA-PET) imaging has emerged as a highly useful tool to localize disease manifestations in PC with a substantial effect on clinical management, especially in cases of low prostate-specific antigen (PSA) values in BCR [7–10].

A recent meta-analysis showed sensitivity to be 42%, 58%, 76%, and 95% at PSA levels of 0–0.2, 0.2–1, 1–2, and >2 ng/mL, respectively [11].

In a previous study, we investigated typical patterns of PC recurrence after RP for patients with BCR in a smaller cohort and found that almost 40% of patients had positive LNs outside the recommended RTOG target volume [12]. In this study, our aim was to validate these results in a large patient cohort and demonstrate typical patterns of recurrence in a color-coded heat map.

Patients and methods

We retrospectively screened 1653 ^{68}Ga-PSMA-PET/CT datasets. These scans were acquired between November 2012 and November 2017 in the Department of Nuclear Medicine at our clinic. A flowchart of the process is depicted in Figure 1. The 233 included patients were initially treated with curative intended RP and lymphadenectomy (LAE) and were referred for ^{68}Ga-PSMA-PET/CT due to the clinical suspicion of tumor recurrence, caused by either rising or persisting PSA levels after surgery.

After tracer injection of ^{68}Ga-PSMA-ligand complex (mean 135 MBq; range 94–211 MBq), contrast-enhanced ^{68}Ga-PSMA-PET/CT imaging was performed using a Biograph mCT scanner (Siemens Medical Solutions). At least two experienced physicians of the department of nuclear medicine performed PET reading and interpretation, followed by a consensus interpretation. A workflow of this protocol and details were published previously [13]. The ^{68}Ga-labeled complex HBED-CC was synthesized as described before [14].

The inclusion and exclusion criteria are presented in Table 1. Androgen-deprivation therapy (ADT) at the time of PSMA-PET imaging was allowed. Within these criteria, 233 patients had a total of 799 LN metastases.

All PET/CT datasets were imported into the planning software (Eclipse 15.6; Varian Medical Systems, Palo Alto, CA, USA), and each LN metastasis was manually contoured on the corresponding CT.

A patient with standard anatomy (average body mass index and no anatomical abnormalities) was selected as a reference. All the contoured LN structures were transferred to the reference CT using rigid and nonrigid image registration techniques. To achieve this, an automated workflow was implemented in MATLAB R2019a (The MathWorks, Inc., Natick, MA, USA): In the first step, the CT data are confined to a threshold ranging between 130 and 2000 Hounsfield units, creating images consisting of bony structures only. With this, rigid and nonrigid registration is performed and the resulting transformation is applied to the patient CT, including the contoured LN structures. In the next step, regions of interest (ROIs) of approximately 7 cm around every single LN are generated onto the transformed patient CT and the reference CT, and nonrigid registration inside the ROIs is performed. Application of this transformation onto the LN contours enables a transfer of the localizations to the reference anatomy.

For nonrigid registration tasks, the B-Spline algorithm of the image registration framework Plastimatch was used, optimizing the mean squared error metric over six stages. All deformed structures on the reference patient were reimported into the treatment planning software, and at least one specialist experienced in radiation oncology assessed each transferred LN with regard to localization and form. Hereby, a three-dimensional atlas with all identified LN localizations on one patient anatomy was created.

In order to evaluate the created data set, binary masks of all transformed structures were generated and summed up to a quantitative atlas representing the spatial distribution of the identified LN localizations. Further, the number of LNs (n = 1–9) in each voxel was represented with color -coding.

LN CTV was contoured according to RTOG guidelines in the standard patient. The RTOG contouring was performed using the guidelines described by Lawton et al [5].

Based on the binary masks of the LN structures and the contoured LN levels, we calculated the overlapping volume (OL) using MATLAB. Thus, we assessed whether they were located within (OL > 90%), partly within (OL 10–90%), or outside (OL < 10%) the RTOG CTV borders.

The underlying method is presented in the study of Borm et al [15]. Not all the included patients were treated with radiation therapy consecutively in the process. The main goal of this study was to detect and visualize patterns of recurrence.

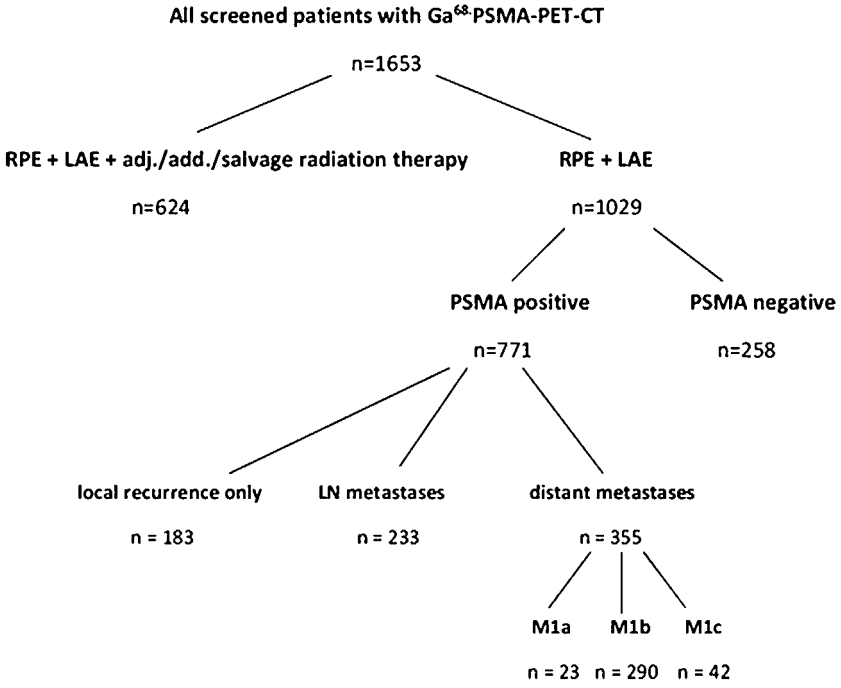

Fig. 1 – Flow chart of screening process. Based on former treatment, patients were divided into two groups and patients with any kind of radiation therapy in the past (*n* = 624) were excluded. Patients with radical prostatectomy (RP) and lymphadenectomy (LAE) only (*n* = 1029) were classified in subgroups according to PSMA-PET/CT diagnosis. In accordance with the defined criteria, 233 patients were included for analysis.
CT = computed tomography; LN = lymph node; PET = positron emission tomography; PSMA = prostate-specific membrane antigen.

Table 1 – Inclusion and exclusion criteria.

Inclusion criteria	Exclusion criteria
≥1 positive lymph node lesion(s) on ^{68}Ga-PSMA-PET/CT (cN1)	No finding on ^{68}Ga-PSMA-PET/CT
	cM1a cranially of renal arteries, cM1b, cM1c
cM1a caudally of the renal arteries	Local recurrence only (according to ^{68}Ga-PSMA-PET/CT)
	Previous pelvic radiation therapy
	PSMA-PET-MR imaging modality

CT = computed tomography; MR = magnetic resonance; PET = positron emission tomography; PSMA = prostate-specific membrane antigen.

In order to illustrate different patterns of LN metastases according to various risk factors, the collective was divided. Stratifications factors included the following: (1) categories of pT (pT ≤ 2c vs pT ≥ 3); (2) initial PSA values (according to the D'Amico risk group classification [16]; <10 vs 10–20 vs >20 ng/mL); (3) PSA values at the time of PSMA-PET imaging (<0.5 vs 0.5–1.0 vs >1 ng/mL); (4) Gleason score ; and (5) The International Society of Urological Pathology (ISUP) grading [17].

Statistical analysis was performed in consultation with a professional statistician and then conducted using IBM SPSS version 26.0 (IBM, Armonk, NY, USA). Spearman's rank correlation was performed to evaluate the impact of different risk factors on the occurrence of LN metastasis in the contemplated areas. The Mann-Whitney *U* test was performed to show significant differences for LNs regarding the defined stratification groups. We assumed statistical significance for $p < 0.05$.

All institutional guidelines were followed. Patients were treated following a consensus of an interdisciplinary tumor board. Informed consent was obtained from all patients. Bavarian state law (Bayrisches Krankenhausgesetz §27 Absatz 4 Datenschutz) allows the use of patient data for research and publication, provided that data related to any person are kept anonymous. German radiation protection laws request a regular analysis of outcomes in the sense of quality control and assurance; thus, in the case of purely retrospective studies, no additional ethical approval is needed under German law.

Results

Overall collective and LN metastasis pattern

Patient characteristics are summarized in Table 2. According to the D'Amico risk group classification, most patients (*n* = 201, 86.3%) had high-risk PC.

In total, 799 LNs were detected by ^{68}Ga-PSMA-PET/CT imaging. The median number of positive LNs per patient was 2 (range 1–22). The average volume of the detected LN lesions was 0.86 cm^3 (median 0.4 cm^3, range 0.01–20 cm^3). The vast majority (70.4%) of patients had three or fewer positive LNs on PSMA-PET imaging; 6.4% of patients had ≥10 positive LNs.

Table 3 gives an overview of LN locations. Almost one-third of all PSMA-positive LNs (*n* = 241, 30.1%) were located along the internal and external iliac arteries, and over half of

Table 2 – Patient characteristics.[a]

Patient characteristics	$n = 233$	%
Tumor stage		
T		
pT1c	1	0.4
T2	67	28.8
pT2a	5	2.1
pT2b	5	2.1
pT2c	51	21.9
pT2x	6	2.7
T3	140	60.0
pT3a	54	23.1
pT3b	78	33.5
pT3x	8	3.4
pT4	2	0.9
pTx	23	9.9
N		
pN0	122	52.4
pN1	77	33.0
pNx	34	14.6
M		
cM0	91	39.0
cM1a	3	1.3
cMx	139	59.7
R		
R0	118	50.6
R1	64	27.5
R2	1	0.4
Rx	50	21.5
Gleason score	203	87.1
5	2	0.9
6	10	4.3
7a	24	10.3
7b	66	28.3
7x	23	9.9
8	26	11.1
9	50	21.4
10	2	0.9
Not available	30	12.9
Initial PSA (ng/mL)	205	88.0
Minimum/maximum (range)	0.6/253 (252.4)	
Mean	19.4	
Standard deviation	28.0	
Median	10.3	
Interquartile range	11.6	
Not available	28	12.0
Age (yr) at the time of PSMA-PET imaging		
Minimum/maximum (range)	48/85 (37)	
Mean	69	
Standard deviation	7.9	
Median	69	
Interquartile range	10.6	
PSA (ng/mL) at the time of PSMA-PET imaging	230	98.7
Minimum/maximum (range)	0.1/16.6 (16.5)	
Mean	2.4	
Standard deviation	3.0	
Median	1.4	
Interquartile range	2.3	
Not available	3	1.3
Time (yr) between RP and PSMA-PET imaging	231	99.1
Minimum/maximum (range)	0.1/19.8 (19.7)	
Mean	4.3	
Standard deviation	4.7	
Median	2.5	
Interquartile range	6.2	
Not available	2	0.9

PET = positron emission tomography; PSA = prostate-specific antigen; PSMA = prostate-specific membrane antigen; RP = radical prostatectomy.
[a] pTx, pNx, Rx, and the Gleason score 7x were defined as such because of missing information.

all LNs ($n = 402$, 50.3%) were accounted for by adding the ones located close to the common iliac arteries.

In Table 3, six LN locations were defined as "others." These LNs were located as follows: two between the musculus obturatorius externus and the musculus pectineus (Fig. 2), between the left musculus obturatorius externus and the musculus piriformis, in the paramedian mesenteric fat tissue of the lower abdomen, between the musculus psoas and the second lumbar vertebra, and another dorsal to the musculus psoas below the aortic bifurcation (Fig. 3).

Figure 4 comprises the total collective to illustrate LN patterns and hot spots with overlapping LNs in a color-coded atlas. Para-aortic hot spots with up to nine LNs can be seen cranial to the standard RTOG CTV radiation field. Further accumulation is visualized along the iliac arteries as well as in the preacetabular areas. A three-dimensional illustration of the LN distribution can be found in Figure 5.

In Table 4, the coverage of LN metastases for all formed subgroups, according to the standard CTV radiation field, is shown. In total, we included 778 of the 799 identified LNs into the atlas, as the algorithm was not able to allocate the remaining 21 LNs (2.6%) appropriately due to anatomical differences. After careful manual revision, these LNs had to be excluded.

In the overall collective, complete coverage by the standard RTOG CTV was accomplished in 31.0% of all LN metastases ($n = 778$). However, more than half were either not (51.8%) or only partially (17.2%) covered. The vast majority of uncovered LNs were situated in the para-aortal as well as in the pelvic region (ie, pararectal, paravesical, preacetabular, presacral, and inguinal; Table 3).

Impact of PSA values at the time of staging (<0.5 vs 0.5–1.0 vs >1.0 ng/mL) on LN metastasis pattern

The median PSA nadir after surgery was 0.09 ng/mL ($n = 117$, mean: 0.51 ng/mL, range 0.01–7.18 ng/ml). The median PSA value at the time of PSMA-PET/CT staging was 1.37 ng/mL ($n = 230$, range 0.11–16.64 ng/ml).

According to Spearman's rank correlation, there is a significant positive correlation between the PSA value at the time of PET/CT and the number of positive LNs ($r = 0.302$, $p < 0.001$, $n = 230$), that is, the higher the PSA, the greater the likelihood of multiple positive LN lesions.

In a logistic regression analysis, the only significant predictor, out of all stratification factors, for detecting LNs outside the standard CTV is the PSA at the time of staging. With increasing PSA, the likelihood of metastases outside the CTV increases (odds ratio = 1.43, 95% confidence interval [1.082–1.872], $p = 0.012$, regression coefficient $B = 0.353$, standard error = 0.14), that is, an increase of 1 ng/mL in PSA raises the risk of metastases outside the CTV by a factor of 1.43.

A color-coded atlas is illustrated in Figure 6 showing visible hot spots with the accumulation of up to eight LNs outside the standard CTV for the group with PSA values >1.0 ng/mL.

Table 3 – Number and location of all PET-positive lymph nodes ($n = 799$).

Location	n	%
Arteria iliaca communis	161	20.2
Arteria iliaca externa	101	12.6
Arteria iliaca interna	140	17.5
Region of the musculus obturatorius internus	34	4.3
Para-aortal/interaortocaval	199	24.9
Pararectal	62	7.8
Paravesical	11	1.4
Preacetabular	19	2.4
Presacral	54	6.8
Retroperitoneal	2	0.3
Inguinal	10	1.3
Other	6	0.8

PET = positron emission tomography.

Impact of ongoing ADT on LN metastasis pattern

At the time of PSMA-PET/CT, ADT was in use in 33 patients (14.2%), while the majority (188 patients, 80.3%) received no ADT. In 12 cases (4.5%), we had no information on ADT intake.

A significant negative correlation was shown between ADT at the time of PET/CT imaging and the number of PSMA-positive LNs (Spearman's rank correlation, $r = -0.224$, $p = 0.001$, $n = 221$). Moreover, ADT and the occurrence of para-aortal LN metastasis showed a significant negative correlation ($r = -0.236$, $p < 0.001$, $n = 221$).

Impact of the tumor stage ≤ pT2c versus ≥ pT3a on LN metastasis pattern

Patients with tumor stage ≤ pT2c showed a significant lower number of PSMA-PET–positive LNs (Mann-Whitney U test, $p = 0.018$). This is confirmed by Spearman's rank correlation, showing a significant positive correlation between the tumor stage and the number of LN metastases observed through PSMA-PET/CT ($r = 0.148$, $p = 0.031$).

Impact of LAE (<10 LN vs ≥10 LN) and time interval between RP and BCR on LN metastasis pattern

In 146 patients (62.7%), information on the precise numerical extent of LAE was present; on average, 17.64 LNs were removed surgically (range 1–88). In

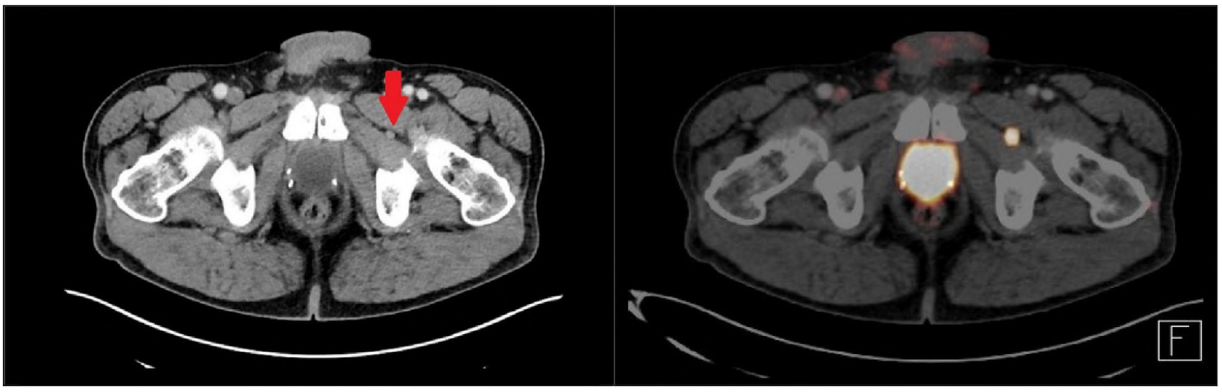

Fig. 2 – PSMA-positive lymph nodes located between the musculus obturatorius externus and the musculus pectineus, (A) marked with an arrow in the patients' CT image and (B) visible through tracer uptake in PSMA-PET/CT.
CT = computed tomography; PET = positron emission tomography; PSMA = prostate-specific membrane antigen.

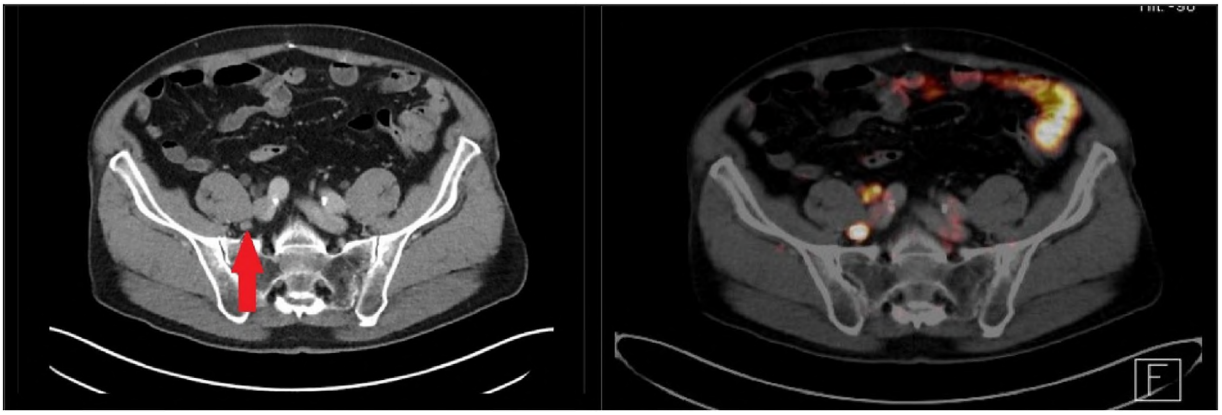

Fig. 3 – PSMA-positive lymph node dorsal to the musculus psoas, (A) marked with an arrow in the patients' CT image and (B) visible through tracer uptake in PSMA-PET/CT.
CT = computed tomography; PET = positron emission tomography; PSMA = prostate-specific membrane antigen.

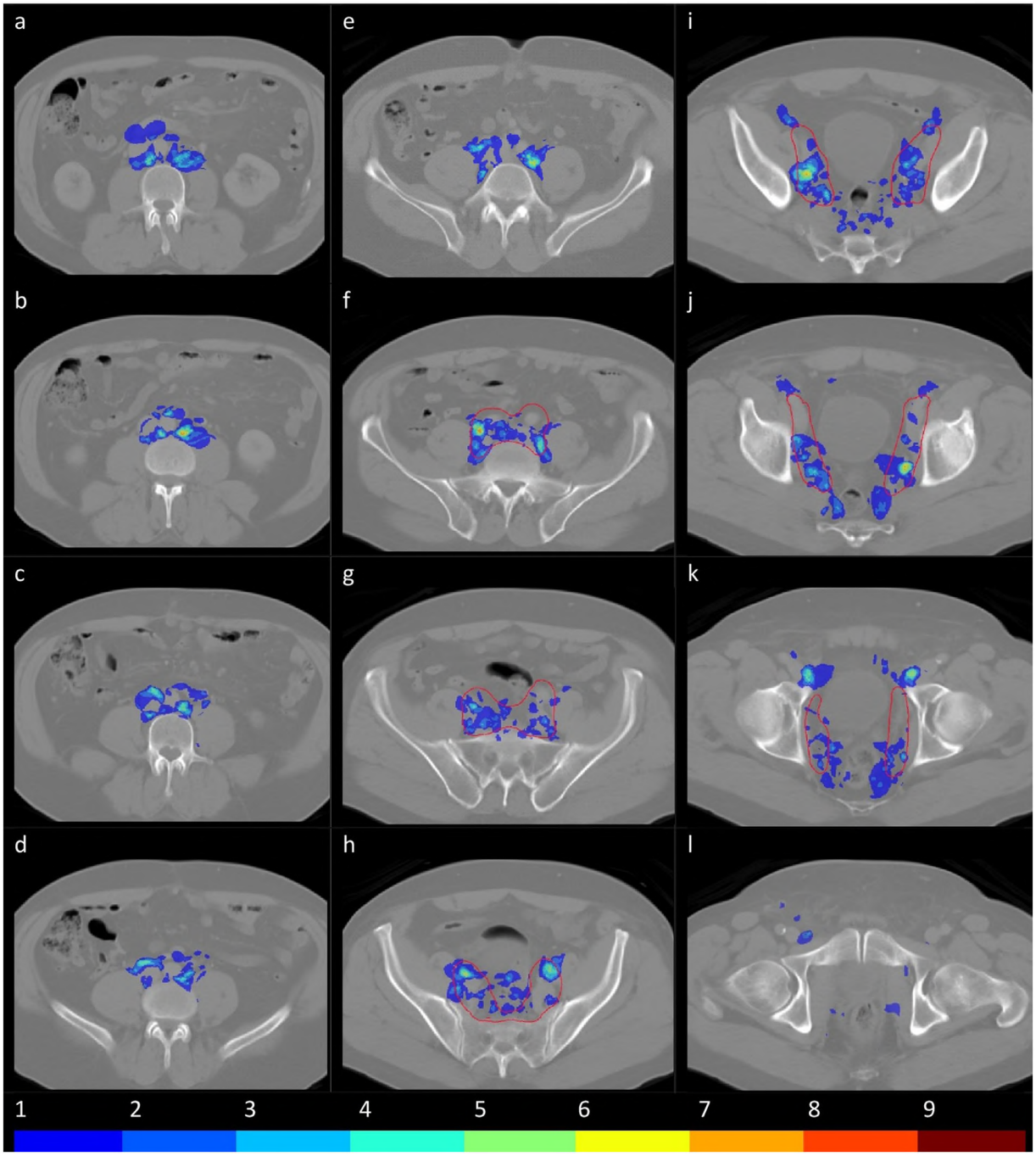

Fig. 4 – Atlas of LN metastasis occurrence ($n = 778$) in the total patients' collective. (A–I) Different slices in 2-cm steps of the standard patients' CT image, showing all identified lymph node lesions. The red line shows the standard clinical target volume radiation field by the Radiation Therapy Oncology Group consensus. Different colors represent the number of accumulating lymph node metastases in several areas.
CT = computed tomography.

113 patients (77.4%), ≥10 LNs were removed, while in 33 patients (22.6%), <10 LNs were resected.

Neither a difference regarding the time interval (RP to recurrence diagnosed by LN metastasis in PSMA-PET/CT) between the two groups (LAE < 10 LNs [3.3 yr, range 0.14–13.7 yr] and LAE ≥ 10 LNs [3.0 yr, range 0.16–11.7 yr]), nor a correlation between the number of LN metastases and the number of removed LNs was found. Yet there was a significant positive correlation between the number of removed LNs during LAE and the likelihood of occurrence of para-aortal metastases (Spearman's rank correlation, $r = 0.110$, $p = 0.018$, $n = 146$).

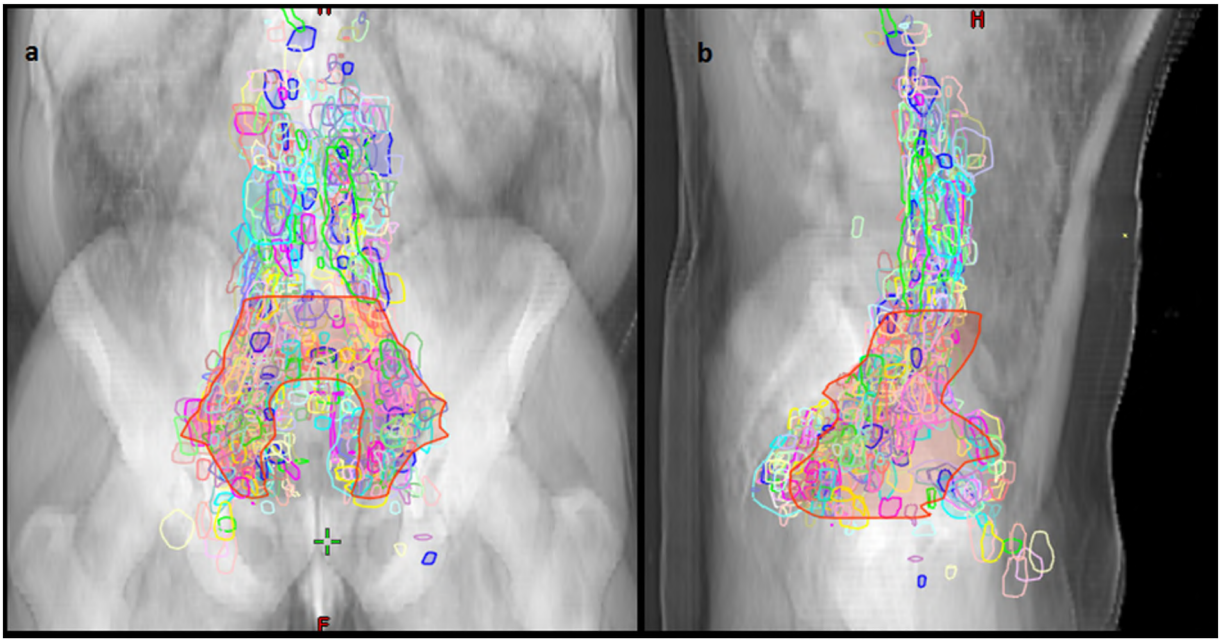

Fig. 5 – Three-dimensional presentation of lymph node metastases ($n = 778$) distribution in the total collective: (A) frontal and (B) sagittal. The red contour outlines the clinical target volume radiation field by Radiation Therapy Oncology Group consensus.

Discussion

To the best of our knowledge, this is the first ^{68}Ga-PSMA-PET/CT–based LN heat map atlas for PC patients with nodal recurrence after RP and LAE. The analysis, including the technique of image registration algorithm to generate a quantitative LN atlas, as well as the mode of illustration, is novel for the generation of a PSMA-based target volume atlas. This approach was initially used to evaluate LN spread in breast cancer patients [15].

The presented data show that, in this predominantly high-risk PC patient cohort, less than one-third of the detected LNs would be covered fully by a standard CTV radiation field according to RTOG contouring guidelines [5], without the additional information of PSMA-PET imaging. Consequently, nearly 70% of the patients' LNs would be treated insufficiently by SRT. These findings are in line with a previously published study from our working group [12]; however, 79% of patients with BCR who had been examined with magnetic resonance lymphography also showed aberrant LN locations [18]. Another study analyzed the location of 209 LN metastases in 87 patients using choline-PET/CT as diagnostic imaging and found 36.8% of PET-positive LNs in a comparable clinical setting to be outside the respective CTV [19]. One likely factor for a higher number in our cohort is the improved sensitivity of PSMA-PET/CT compared with choline-PET/CT [20,21]. Additionally, our predominantly high-risk collective may also explain different results of LN coverage.

Further, Boreta et al [22] identified 66 patients with 70 ^{68}Ga-PSMA-PET–positive LNs, from which 25 LNs (35.7%) were located outside the standard radiation field. The collective here was somewhat different, recruiting exclusively patients with PSA values $\leq$2.0 ng/mL but also with M1b disease.

Although the inclusion criteria as well as diagnostic tools vary, the main message remains: standard CTVs are not suited for all patients, representing one likely cause of SRT failure.

There are two obvious options to solve this problem. One is to screen all high-risk PC patients in a salvage treatment approach with PSMA-PET imaging, in order to minimize the chances of missing the actual site of recurrence. The other is to improve target volume guidelines, based on increasingly gathered data and novel imaging techniques. Possibly the volumes would differ, depending on the patients' risk factors, individualizing each treatment volume without the need of further imaging.

Despite the fact that PSMA-PET–based staging has become widely available, there are factors limiting its use. With this study, we aimed to identify risk factors to predict the probability of LN metastases in unusual locations and to help in the decision process on whether PSMA-PET imaging is necessary for salvage therapy staging.

Our results clearly suggest that the PSA at the time of PET imaging has the best predictive value on the distribution pattern of LN metastases. In patients with PSA values $>$1.0 ng/mL, complete coverage was reached in only slightly more than one-quarter of LNs examined. Additionally, every increase of 1 ng/mL in PSA raises the risk of metastases outside the CTV by a factor of 1.43. We conclude that especially high PSA values ($>$1.0 ng/mL) increase the probability of LN metastases outside a standard radiation field and therefore justify further diagnostic imaging via

Table 4 – Coverage (in percentage of its volume) of lymph node metastases by a standard clinical target volume radiation field after the Radiation Therapy Oncology Group consensus statement.

n (patients)	*n* (lymph nodes)	Not covered (<10%) LN, *n* (%)	Partially covered (10–90%) LN, *n* (%)	Completely covered (>90%) LN, *n* (%)
All patients		403 (51.8)	134 (17.2)	241 (31.0)
233	778			
iPSA (ng/mL)				
<10		162 (52.8)	52 (16.9)	93 (30.3)
101	307			
10–20		111 (53.1)	33 (15.8)	65 (31.1)
61	209			
>20		57 (42.5)	29 (21.7)	48 (35.8)
43	134			
pT				
<pT2		86 (51.8)	33 (19.9)	47 (28.3)
68	166			
>pT3		278 (53.2)	84 (16.0)	161 (30.8)
142	523			
PSA at the time of PSMA-PET imaging (ng/mL)				
<0.5				
51	87	35 (40.2)	16 (18.4)	36 (41.4)
0.5–1.0				
44	110	37 (33.6)	21 (19.1)	52 (47.3)
>1.0				
135	564	323 (57.3)	94 (16.7)	147 (26.0)
ISUP				
1		28 (58.3)	7 (14.6	13 (27.1)
12	48			
2		28 (53.9)	11 (21.1)	13 (25.0)
24	52			
3		116 (53.9)	35 (16.3)	64 (29.8)
66	215			
4		35 (50.7)	8 (11.6)	26 (37.7)
26	69			
5		92 (50.0)	29 (15.8)	63 (34.2
52	184			
LAE				
<10		49 (49.0)	24 (24.0)	27 (27.0)
33	100			
>10		182 (52.0	49 (14.0)	119 (34.0)
113	350			

ISUP = International Society of Urological Pathology; LAE = lymphadenectomy; LN = lymph node; PET = positron emission tomography; PSA = prostate-specific antigen; PSMA = prostate-specific membrane antigen.

PSMA-PET/CT. This is supported by previous studies that also revealed a high impact of the PSA value at the time of imaging on whether LNs can be suspected inside or outside the radiation field [18,23].

In our study, a high PSA value was associated with both a higher rate of scan positivity and a higher chance of extrapelvic LN metastases. This result might leave clinicians in a state of discrepancy; on the one hand, SRT should not be delayed [24–26] by waiting for higher PSA values to increase the chance of correlates upon imaging, and on the other hand, SRT with standard radiation therapy fields has a considerable chance of missing the target. Aside from the PSA, there are other evolving possibilities such as genomic risk classifiers to predict advanced or metastasized PC stages [27].

Further, there was a noticeable relation between pT stages and the number of positive LN metastases: the higher the tumor stage, the greater the likelihood of more than one LN metastasis. This is a predescribed circumstance in the primary setting [28] and can be confirmed in our collective in a salvage setting.

In our cohort, we found moderately different numbers of LNs covered by CTV regarding the extent of the earlier conducted LAE (full coverage: LAE $\geq$ 10: 34.0% vs LAE < 10: 27.0%), while the mean time interval between LAE and diagnosis of recurrence was comparable.

As a standard procedure, extended LAE at our institution is performed in intermediate- and high-risk patients, including the obturatoric as well as internal, external, and common iliac nodes [29]. Since there are differences between institutions and surgeons, interindividual adjustments in LAE are likely in our collective, which contains RPs undertaken at different institutions.

We hypothesized that the surgical intervention of LAE may change the physiological lymph drainage routes after surgery, and we therefore questioned whether to expect more LNs in extraordinary locations depending on the extension of LAE and the respective LNs removed [30]. This

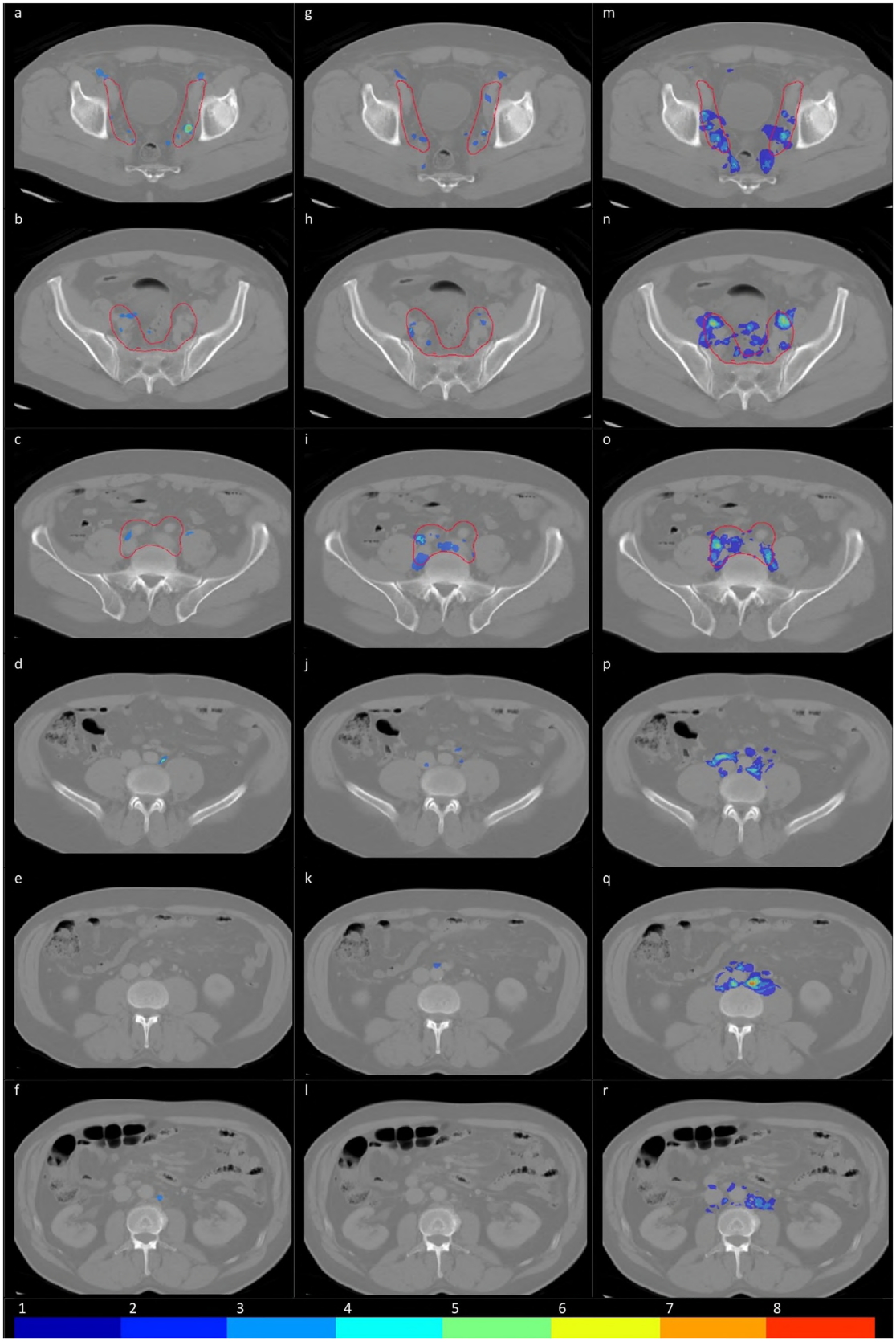

Fig. 6 – Distribution of lymph node metastases in relation to the PSA value (in ng/mL) at the time of PSMA-PET/CT diagnosis in color coding. (A–F) Different slices of the lymph node atlas from all patients with PSA values of <0.5 ng/mL. (G–L) Corresponding slices for the group with PSA values between 0.5 and 1.0 ng/mL. (M–R) The group with PSA values >1.0 mg/dl. The color code shows the number of accumulating lymph nodes in one location. The standard clinical target volume radiation field is contoured as the red line.
CT = computed tomography; PET = positron emission tomography; PSA = prostate-specific antigen; PSMA = prostate-specific membrane antigen.

assumption is supported by the finding that the higher the number of LNs removed during surgery, the higher the chance of para-aortal LN metastases, suggesting that once multiple LNs in the pelvic region are surgically removed, the recurrent tumor cells might have quicker access to the para-aortal region. It is probably fair to say that lymph drainage routes oftentimes are more complex than they might have been anticipated [31,32].

There are limitations to this study: PSMA-PET/CT itself served as the diagnostic gold standard, meaning that the PET-positive findings in this study lack histopathological confirmation. A former lesion-based analysis of sensitivity, specificity, negative predictive value, and positive predictive value revealed values of 76.6%, 100%, 91.4%, and 100 %, respectively [7]. In addition, PSMA-PET/CT reading is afflicted by insecurities. Lastly, the morphing process comprises inaccuracies due to being in a state of fine-tuning and development.

Conclusions

We developed the first LN atlas for patients with recurrent PC using a heat map technique. It illustrates typical patterns of involvement in a cohort of mainly high-risk patients and presents hot spots of LN metastases. Decisive for SRT is that the vast majority (69%) of the detected LNs in the whole collective are insufficiently, or not at all, covered by a standard RTOG CTV.

PSA at the time of PET/CT imaging had the highest predictive value on the distribution pattern of LN metastases. An increase of 1 ng/mL in PSA raises the risk of metastases outside the CTV by a factor of 1.43.

In order to avoid missing the target and to improve PC patients' outcomes in an SRT approach, PSMA-PET/CT imaging should strongly be considered for tailoring treatment planning, especially for patients with a PSA value of >1 ng/mL. We suggest focusing on the individualization of SRT volumes for high-risk PC patients in future studies, as the application of the standard RTOG CTV for pelvic irradiation is inadequate in most of the cases.

Author contributions: Kilian Schiller had full access to all the data in the study and takes responsibility for the integrity of the data and the accuracy of the data analysis.
Study concept and design: Schiller, Stöhrer, Düsberg, Devecka, Borm, Duma, Combs.
Acquisition of data: Schiller, Stöhrer, Düsberg, Devecka, Rauscher, Eiber.
Analysis and interpretation of data: Schiller, Stöhrer, Düsberg, Devecka, Tauber, Heck, Gschwend, Duma, Combs.
Drafting of the manuscript: Schiller, Stöhrer.
Critical revision of the manuscript for important intellectual content: Schiller, Stöhrer, Vogel, Heck, Gschwend.
Statistical analysis: Stöhrer.
Obtaining funding: None.
Administrative, technical, or material support: Düsberg, Devecka, Combs.
Supervision: Gschwend, Duma, Combs.
Other: None.

Financial disclosures: Kilian Schiller certifies that all conflicts of interest, including specific financial interests and relationships and affiliations relevant to the subject matter or materials discussed in the manuscript (eg, employment/affiliation, grants or funding, consultancies, honoraria, stock ownership or options, expert testimony, royalties, or patents filed, received, or pending), are the following: None.

Funding/Support and role of the sponsor: None.

References

[1] Ferlay J, Soerjomataram I, Dikshit R, et al. Cancer incidence and mortality worldwide: sources, methods and major patterns in GLOBOCAN 2012. Int J Cancer 2015;136:E359–86.
[2] Hull GW, Rabbani F, Abbas F, Wheeler TM, Kattan MW, Scardino PT. Cancer control with radical prostatectomy alone in 1,000 consecutive patients. J Urol 2002;167(2 Pt 1):528–34.
[3] Kupelian P, Katcher J, Levin H, Zippe C, Klein E. Correlation of clinical and pathologic factors with rising prostate-specific antigen profiles after radical prostatectomy alone for clinically localized prostate cancer. Urology 1996;48:249–60.
[4] Stephenson AJ, Scardino PT, Eastham JA, et al. Postoperative nomogram predicting the 10-year probability of prostate cancer recurrence after radical prostatectomy. J Clin Oncol 2005;23:7005–12.
[5] Lawton CAF, Michalski J, El-Naqa I, et al. RTOG GU radiation oncology specialists reach consensus on pelvic lymph node volumes for high-risk prostate cancer. Int J Radiat Oncol Biol Phys 2009;74:383–7.
[6] Rouvière O, Vitry T, Lyonnet D. Imaging of prostate cancer local recurrences: why and how? Eur Radiol 2010;20:1254–66.
[7] Afshar-Oromieh A, Avtzi E, Giesel FL, et al. The diagnostic value of PET/CT imaging with the 68Ga-labelled PSMA ligand HBED-CC in the diagnosis of recurrent prostate cancer. Eur J Nucl Med Mol Imaging 2015;42:197–209.
[8] Eiber M, Maurer T, Souvatzoglou M, et al. Evaluation of hybrid (6)(8) Ga-PSMA ligand PET/CT in 248 patients with biochemical recurrence after radical prostatectomy. J Nucl Med 2015;56:668–74.
[9] van Leeuwen PJ, Stricker P, Hruby G, et al. 68Ga-PSMA has a high detection rate of prostate cancer recurrence outside the prostatic fossa in patients being considered for salvage radiation treatment. BJU Int 2016;117:732–9.
[10] De Visschere PJL, Standaert C, Futterer JJ, et al. A systematic review on the role of imaging in early recurrent prostate cancer. Eur Urol Oncol 2019;2:47–76.
[11] Perera M, Papa N, Christidis D, et al. Sensitivity, specificity, and predictors of positive (68)Ga-prostate-specific membrane antigen positron emission tomography in advanced prostate cancer: a systematic review and meta-analysis. Eur Urol 2016;70:926–37.
[12] Schiller K, Sauter K, Dewes S, et al. Patterns of failure after radical prostatectomy in prostate cancer—implications for radiation therapy planning after (68)Ga-PSMA-PET imaging. Eur J Nucl Med Mol Imaging 2017;44:1656–62.
[13] Eiber M, Weirich G, Holzapfel K, et al. Simultaneous 68Ga-PSMA HBED-CC PET/MRI improves the localization of primary prostate cancer. Eur Urol 2016;70:829–36.
[14] Eder M, Schafer M, Bauder-Wust U, et al. 68Ga-complex lipophilicity and the targeting property of a urea-based PSMA inhibitor for PET imaging. Bioconjug Chem 2012;23:688–97.
[15] Borm KJ, Voppichler J, Dusberg M, et al. FDG/PET-CT-based lymph node atlas in breast cancer patients. Int J Radiat Oncol Biol Phys 2019;103:574–82.
[16] D'Amico AV, Whittington R, Malkowicz SB, et al. Biochemical outcome after radical prostatectomy, external beam radiation therapy,

or interstitial radiation therapy for clinically localized prostate cancer. JAMA 1998;280:969–74.

[17] Epstein JI, Egevad L, Amin MB, Delahunt B, Srigley JR, Humphrey PA. The 2014 International Society of Urological Pathology (ISUP) consensus conference on Gleason grading of prostatic carcinoma: definition of grading patterns and proposal for a new grading system. Am J Surg Pathol 2016;40:244–52.

[18] Meijer HJM, van Lin EN, Debats OA, et al. High occurrence of aberrant lymph node spread on magnetic resonance lymphography in prostate cancer patients with a biochemical recurrence after radical prostatectomy. Int J Radiat Oncol Biol Phys 2012;82:1405–10.

[19] Hegemann N-S, Wenter V, Spath S, et al. Distribution of prostate nodes: a PET/CT-derived anatomic atlas of prostate cancer patients before and after surgical treatment. Radiat Oncol 2016;11:37.

[20] Schwenck J, Rempp H, Reischl G, et al. Comparison of (68)Ga-labelled PSMA-11 and (11)C-choline in the detection of prostate cancer metastases by PET/CT. Eur J Nucl Med Mol Imaging 2017;44:92–101.

[21] Bluemel C, Krebs M, Polat B, et al. 68Ga-PSMA-PET/CT in patients with biochemical prostate cancer recurrence and negative 18F-choline-PET/CT. Clin Nucl Med 2016;41:515–21.

[22] Boreta L, Gadzinski AJ, Wu SY, et al. Location of recurrence by gallium-68 PSMA-11 PET scan in prostate cancer patients eligible for salvage radiotherapy. Urology 2019;129:165–71.

[23] Verburg FA, Pfister D, Heidenreich A, et al. Extent of disease in recurrent prostate cancer determined by [(68)Ga]PSMA-HBED-CC PET/CT in relation to PSA levels, PSA doubling time and Gleason score. Eur J Nucl Med Mol Imaging 2016;43:397–403.

[24] Stish BJ, Pisansky TM, Harmsen WS, et al. Improved metastasis-free and survival outcomes with early salvage radiotherapy in men with detectable prostate-specific antigen after prostatectomy for prostate cancer. J Clin Oncol 2016;34:3864–71.

[25] Tendulkar RD, Agrawal S, Gao T, et al. Contemporary update of a multi-institutional predictive nomogram for salvage radiotherapy after radical prostatectomy. J Clin Oncol 2016;34:3648–54.

[26] DGU. Interdisziplinäre Leitlinie der Qualität S3 zur Früherkennung, Diagnose und Therapie der verschiedenen Stadien des Prostatakarzinoms. Version 5.1. 2019.

[27] Xu MJ, Kornberg Z, Gadzinski AJ, et al. Genomic risk predicts molecular imaging-detected metastatic nodal disease in prostate cancer. Eur Urol Oncol 2019;2:685–90.

[28] Faul P, Eisenberger F, Elsasser E. [Metastatic involvement of pelvic lymph nodes in relation to the morphological differentiation grade and clinical status of prostatic cancer.]. Der Urologe Ausg A 1985;24:326–9.

[29] Mottet N, Bellmunt J, Bolla M, et al. EAU-ESTRO-SIOG guidelines on prostate cancer. Part 1: screening, diagnosis, and local treatment with curative intent. Eur Urol 2017;71:618–29.

[30] Vermeeren L, Meinhardt W, van der Poel HG, Valdes Olmos RA. Lymphatic drainage from the treated versus untreated prostate: feasibility of sentinel node biopsy in recurrent cancer. Eur J Nucl Med Mol Imaging 2010;37:2021–6.

[31] Sivaraman A, Benfante N, Touijer K, et al. Can pelvic node dissection at radical prostatectomy influence the nodal recurrence at salvage lymphadenectomy for prostate cancer? Invest Clin Urol 2018;59:83–90.

[32] Nguyen DP, Huber PM, Metzger TA, Genitsch V, Schudel HH, Thalmann GN. A specific mapping study using fluorescence sentinel lymph node detection in patients with intermediate- and high-risk prostate cancer undergoing extended pelvic lymph node dissection. Eur Urol 2016;70:734–7.